Sequential model to describe the nicotinic synaptic current

H. Parnas, M. Flashner, and M. E. Spira
The Otto Loewi Center for Cellular and Molecular Neurobiology and the Department of Neurobiology, The Hebrew University of Jerusalem, Israel 91904

ABSTRACT An analytical formula is derived to describe the synaptic end plate current (epc) at the nicotinic receptor. Various concurrently occuring underlying processes, including (*a*) diffusion, (*b*) hydrolysis of acetylcholine, and (*c*) its binding to the dimeric receptor, were considered in order to develop the equation. Numeric solution of the equations that describe the events underlying the epc showed that these events occur in sequence, rather than concurrently. This sequential occurence of the processes allowed for simplifications, which were used as the basis for the new description of the epc. The resulting formula serves as a tool for evaluating the relative contribution of the various processes in formation of the natural occuring transient epc.

INTRODUCTION

The molecular events underlying the generation of the post-synaptic end plate current (epc) at the nicotinic receptor are now well understood. Several mathematical models have been suggested to describe these events (Kordas, 1977; Rosenberry, 1979; Wathey et al., 1979; Land et al., 1984). The models, though differing in some aspects, all describe the synaptic current as an outcome of several concomitant occuring events. As a result, the epc is obtained by a numerical solution of the corresponding differential equations.

These numerical techniques provide highly precise descriptions of postsynaptic responses. However, analytical solutions can offer additional insight into the component mechanisms of the epc, such as amplitude, rise time, and decay rate. These, in turn, may be used to evaluate the underlying rate constants.

Here, we shall derive a simple, analytical description of the epc, which is in some ways similar to the approach of Magleby and Stevens (1972). The method requires certain simplifying assumptions to be made, which, in the end, sacrifice some precision in the simulation of the epc. Throughout the derivation, we will attempt to maintain reasonable agreement between the full numerical solutions and the analytical expressions. Reasonable agreement shall thus be defined as that exhibiting qualitatively similar behavior within the same order of magnitude. We will show that the analytical expression for the epc indeed yields information about the relative sensitivity of the epc to variations in the magnitudes of the rate constants and concentrations of the participating components. In particular, the analytical solution will demonstrate that the peak amplitude of the synaptic current shows a sigmoidal dependence upon transmitter concentration, as expected from the molecular mechanism of channel opening. Also, the rising phase of the epc will be shown to be dependent upon several parameters, among them the rate constants of channel opening and closing, but also the rate of dissociation of the second molecule of transmitter from the receptor. An understanding of these and other qualitative features of the epc reveals which of the parameters have the lesser role in determining the epc, and which have a negligible effect. Such an understanding is difficult to achieve via numerical solutions, which are primarily aimed at achieving maximal precision.

Description of the events that underlie the synaptic current

We concentrate here on nicotinic cholinergic synapses. We assume, as others before (e.g., Magleby and Stevens, 1972; Rosenberry, 1979), that the synaptic current, epc, is directly proportional to the number of open channels. Here, we present a description for the kinetics of channel opening, hence for the miniature end plate currents, mepc. Up to a certain, high range, the epc is a sum of mepcs (Mclachlan and Martin, 1981). Hence, the expression derived to describe the mepc can be applied to describe the epc.

The events underlying the synaptic current are as follows (Rosenberry, 1979; Land et al., 1984; Wathey et al., 1979): (*a*) The released acetylcholine, A, diffuses radially in the volume adjacent to the post-synaptic membrane. (*b*) A is hydrolyzed by acetylcholine esterase, E, according to scheme 1:

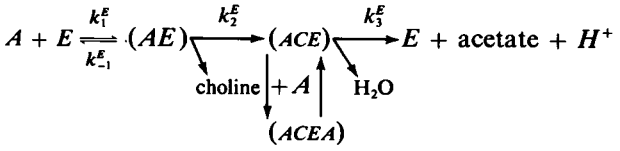

Scheme 1

0006-3495/89/05/875/10 $2.00

As can be seen in (scheme 1), the hydrolysis of A involves three steps. In the first, the complex (AE) is formed. (AE) then undergoes changes that result in the formation of the next complex (ACE), while choline is liberated. The complex ACE can either bind another A to form the additional complex ($ACEA$), or be hydrolyzed to give the final product, acetate. Rosenberry and Bernhard (1972) showed that the rate of binding of A to (ACE) is ~100-fold slower than the rate of binding of A to the enzyme E. The former step can therefore be neglected in the following discussion.

(c) An additional event that seems to occur concurrently with the hydrolysis, is the binding of A to the (dimeric) cholinergic receptors, R. As a result ionic channels are opened. Thus,

$$A + R \underset{k_{-1}^R}{\overset{2k_1^R}{\rightleftharpoons}} (AR)$$

$$(AR) + A \underset{2k_{-2}^R}{\overset{k_2^R}{\rightleftharpoons}} (A_2R)$$

$$(A_2R) \underset{k_c}{\overset{k_o}{\rightleftharpoons}} O$$

Scheme 2

According to scheme 2, R binds two molecules of A, each with the same rate constant (Land et al., 1984). That is, the binding to R does not show a cooperative dependence on A. The coefficient "2" in (scheme 2a) is the standard statistical factor associated with a dimer. The dissociation constants have been treated similarly. k_o is the rate of opening, while k_c is the rate of closing the channels.

The differential equations, based on schemes 1 and 2, which should be solved in order to describe the kinetics of the synaptic current, epc, are as follows:

$$dO/dt = k_o(A_2R) - k_cO \quad (1)$$

$$d(A_2R)/dt = k_2^R(AR) \cdot A - (A_2R)[2k_{-2}^R + k_o] + k_cO \quad (2)$$

$$d(AR)/dt = 2k_1^R \cdot A \cdot R - (AR)[k_2^R \cdot A + k_{-1}^R] + 2k_{-2}^R(A_2R) \quad (3)$$

$$dA/dt = -k_1^E \cdot A \cdot E - 2k_1^R \cdot A \cdot R - k_2^R(AR) \cdot A + k_{-1}^E(AE) + 2k_{-2}^R(A_2R) + k_{-1}^R(AR) \quad (4)$$

$$d(AE)/dt = k_1^E \cdot A \cdot E - (AE)[k_{-1}^E + k_2^E] \quad (5)$$

$$d(ACE)/dt = k_2^E(AE) - k_3^E(ACE). \quad (6)$$

In addition, there are two conservation laws:

$$R = R_T - (AR) - (A_2R) - O \quad (7a)$$

$$E = E_T - (AE) - (ACE), \quad (7b)$$

where R_T and E_T are the total concentration of R and E, respectively.

One simplification can immediately be carried out. Comparison of k_2^E and k_3^E (Table 1) shows that $k_3^E \gg k_2^E$. As a consequence, the formation of (ACE) can be neglected. The hydrolysis of A can then be written in the conventional way,

$$A + E \underset{k_{-1}^E}{\overset{k_1^E}{\rightleftharpoons}} AE \xrightarrow{k_2^E} \text{Acetate} + H^+ + E,$$

and Eq. 6 can be omitted.

Because of the concurrent action of A in Eqs. 2–4, it is highly doubtful that Eqs. 1–7 can be solved analytically in their present form. As will be seen later, we will suggest a procedure with the outcome of a manageable analytical formula for the epc. Toward this end, Eqs. 1–7 are first solved numerically, and the temporal behavior of the underlying components is analyzed. The temporal behavior of the various components depends strongly on the values of the corresponding rate constants. We therefore used values that were taken from the literature as listed in Table 1. These values were previously used by the various authors (see Table 1) to simulate numerically the synaptic current.

In order to evaluate the initial concentration of Ach, A, a discussion concerning Ach diffusion is required. Following previous authors (Rosenberry, 1979; Matthews-Bellinger and Salpeter, 1978; Miledi et al., 1984), we assume instantaneous secretion of Ach onto the post-synaptic "critical zone" (e.g., the post-synaptic membrane adjacent to a release site in which the receptors, R, are concentrated). Assuming a diffusion coefficient of 10^{-5} cm^2/s and a critical zone of $0 \cdot 3$ μm^2 (Rosenberry, 1979), it will only take ~10 μs for A to diffuse throughout

TABLE 1 Values and the corresponding references of the rate constants that have been used for the simulation of the synaptic current

Parameter	Value	Reference
k_1^E	$2 \cdot 10^8$ M^{-1} s^{-1}	Rosenberry, 1975
k_1^E	10^3 s^{-1}	
k_2^E	$1.1 \cdot 10^5$ s^{-1}	Rosenberry, 1979
k_3^E	$2 \cdot 10^4$ s^{-1}	Miledi et al., 1984
		Rosenberry, 1975
k_1^R	$3 \cdot 10^7$ M^{-1} s^{-1}	Land et al., 1984
k_1^R	10^4 s^{-1}	Land et al., 1984
k_2^R	$3 \cdot 10^7$ m^{-1} s^{-1}	Land et al., 1984
k_2^R	10^4 s^{-1}	Land et al., 1984
k_o	$2 \cdot 10^4$ s^{-1}	Land et al., 1984
k_c	$5 \cdot 10^3$ s^{-1}	Land et al., 1984

The values of k_{-1}^R and k_{-2}^R that we have used are higher (twofold) than the ones used by Land et al. (1984). In the absence of information concerning k_{-1}^E, an arbitrary low value has been chosen.

the critical zone. We therefore assume that A is uniformly distributed throughout the critical zone before the events leading to the formation of the epc take place. Later, due to the uniform concentration, diffusion of A out of the critical zone becomes negligible in comparison to the fast hydrolysis of Ach. The concentration of A was indeed shown to be rather uniform throughout the critical zone (Matthews-Bellinger and Salpeter, 1978). The initial value of A, A_0, and the total concentrations of R and E R_T and E_T, respectively, are depicted in Table 2. Note that R_T and E_T are used in concentration and not in density units. The transfer procedure from density to concentration units is described in Table 2.

Fig. 1 shows a computer simulation of the synaptic current using the differential Eqs. 1–7 and the parameters listed in Tables 1 and 2. The resulting synaptic current is consistent with experimental results. Thus, the time of the peak amplitude is ~100 μs, in accordance with experimental results (Magleby and Stevens, 1972; Gage and McBurney, 1975). Moreover, the decay is exponential (see insert in Fig. 1) and the decay constant is 2 · 2 ms^{-1}. Similar values were obtained experimentally by Magleby and Stevens, 1972 (i.e., 1.5 ms^{-1} – 2 ms^{-1} for positive membrane potentials). It also agrees with the value of 1.6 ms^{-1} that has been observed in eel electroplaques (Sheridan and Lester, 1977) and is somewhat higher than the values obtained in frog junctions (0.6 ms^{-1}, Anderson and Stevens, 1973) and in toad junctions (0.5 ms^{-1}, Gage and McBurney, 1975). Finally, the maximum number of open channels at the peak of the epc corresponds to ~7 · 10^{-5} M (see Fig. 1). This value corresponds to ~5% of the total initial concentration of acetylcholine. This is in reasonable agreement with the 10% estimation of Colquhoun (1975). The values of the rate constants used in the simulation of Fig. 1 can be compared with the corresponding values estimated from single-channel measurements (Colquhoun and Sakmann, 1985). Accordingly, the value of 2 · $10^4 s^{-1}$ for k_o, the rate constant of opening the channel, agrees well with the observed value of 3 · $10^4 s^{-1}$. A larger difference is observed with respect to the rate constant of channel closure, k_c. We have used, after Land et al. (1984), a value of 5 · $10^3 s^{-1}$, while Colquhoun and Sakmann (1985) reported a value of 7 · $10^2 s^{-1}$.

For clarity and brevity, we will refer in later discussion to the solution of Eqs. 1–7 and their presentation in Fig. 2 as the "continuous approach."

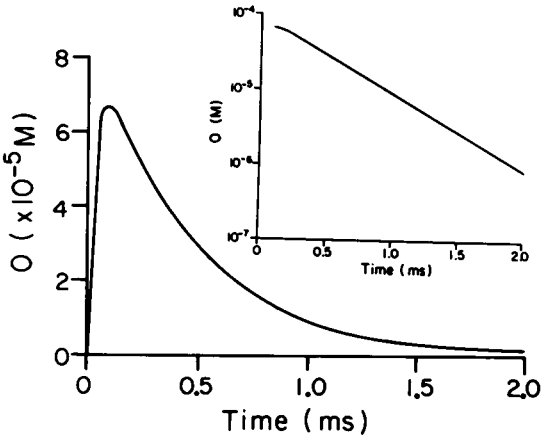

FIGURE 1 Computer simulation of O using Eqs. 1–7, excluding Eq. 6. Parameters given in Tables 1 and 2. (*Insert*), semilogarythmic plot of the decaying phase of O. The decay constant is 2.2 ms^{-1}. In this and in the following figures, t = 0 is taken at the time at which ACh concentration equilibrates in the synaptic cleft.

TABLE 2 Values of the concentrations of A_0, E_T, and R_T are used for the simulation of the synaptic currents

Parameter	Value	Reference
A_0	2 · 10^{-3} M	Matthews-Bellinger and Salpeter., 1978
E_T	6 · 10^{-4} M	Miledi et al., 1984
R_T	6 · 10^{-4} M	Bernard et al., 1973

E_T, R_T, and A_0 are calculated in units of concentration. We used the transformation factor from surface density to concentration, as developed by Wathey et al. (1979). Accordingly, 30,000 molecules per μm^2 correspond to 1 mM.

The following calculations are based on this transformation factor: (*a*) Concentration of A_0. The area that the content of a vesicle occupies following ~10 μs of diffusion is ~0.3 μm^2, the area of the critical zone. Therefore, if 10^3 molecules spread in 0.3 μm^2, according to the transformation factor introduced above, $A_0 \approx 10^{-3}$ M. Examination of Fig. 2 in Matthews-Bellinger and Salpeter (1978) shows that a more exact value for A_0 is 2 · 10^{-3} M. We therefore used the last one. (*b*) Concentration of R_T. According to Bernard et al. (1973), the total number of receptors per site is 3 · 10^7. Because the total postsynaptic area per end plate is ~1,500 μm^2 (Matthews-Bellinger and Salpeter, 1978), it follows that the surface density of receptors is 2 · $10^4/\mu m^2$. Using the above mentioned transformation factor, R_T = 6 · 10^{-4} M. (*c*) Concentration of E_T. We assume, as does Bernard et al. (1973) and Rosenberry (1979), that the density of AChE is about the same as that of the receptors. Therefore we assume the same concentration of E_T as that of R_T.

SEQUENTIAL MODEL TO DESCRIBE SYNAPTIC CURRENT

Justification for the sequential approach

In view of the adequate agreement of the simulation with experimental results, we decided to examine in detail the temporal behavior of the various components. The results are depicted in Fig. 2. We observe that the various reactions do in fact occur in sequence, rather than simultaneously. The first reaction in the sequence is the hydrolysis of A. The peak of AE occurs in ~5 μs (Fig. 2, *B* and

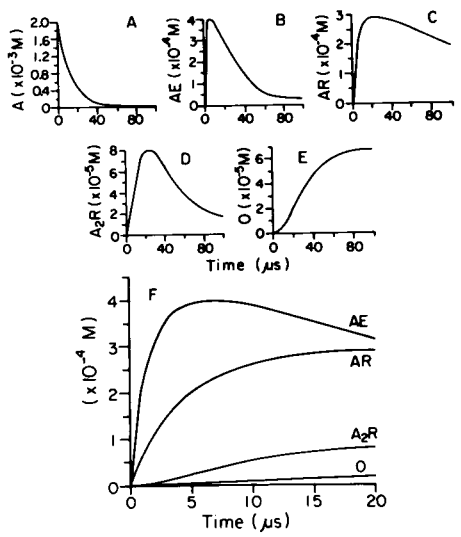

FIGURE 2 Computer simulation of A, AE, AR, A_2R, and O using Eqs. 1–7. Note the difference in time scale of F compared with A–E. The time scale was chosen to illustrate the sequential occurence of the various components.

F). At that time, the next reaction in the sequence, binding of A to R, has not reached its peak. Moreover, at the peak of AE, (AR) is only half the level of (AE). The complex (AR), the second reaction in the chain, reaches its peak at ~20 μs (Fig. 2 C). At the time of the peak of (AR), the third event, i.e., formation of the complex (A_2R), still lags (Fig. 2 F). In addition, at the time of the build-up of A_2R, (AR), which has already reached its peak, remains rather constant (compare Fig. 2, C and D). Finally, the last event is the opening of the channels, that is, the accumulation of O. This is still negligible when (AE) and (AR) are already decaying (compare Fig. 2, B, C, and E). O also lags significantly behind A_2R. The peak of O is obtained at 100 μs (Fig. 2 E), while (A_2R) reaches its peak after ~30 μs.

The sequential occurence of the various reactions enables for the rewriting of Eqs. 1–7 as a set of sequential equations with minimal interaction among the various reactions.

Formulating the sequential approach

Fig. 2 shows that the first reaction in the chain is the hydrolysis of A. Therefore, initially (for a period of ~7–10 μs), one can approximate Eq. 4 by,

$$dA/dt = k_1^E \cdot A \cdot E + k_{-1}^E(AE). \tag{8}$$

In other words, during 7–10 μs, A disappears due to hydrolysis only.

In addition, (ACE) can be neglected in Eq. 7b, giving

$$E = E_T - (AE). \tag{9}$$

Simplification of Eq. 3, the (AR) reaction, can be achieved, because the contribution of the term $2k_{-2}^R(A_2R)$ to the build-up of (AR) is small compared with the contribution of $k_1^R A \cdot R$ (see Fig. 2 F). Thus, Eq. 3 becomes,

$$d(AR)/dt = 2k_1^R \cdot A \cdot R - (AR)[k_2^R \cdot A + k_1^R]. \tag{10}$$

The next reaction, formation of (A_2R), can also be simplified according to the same pattern. Fig. 2 shows that as (A_2R) builds up, O is still small. Therefore, Eq. 2 can be approximated by,

$$d(A_2R)/dt = k_2^R(AR) \cdot A - (A_2R)[2k_2^R \cdot A + k_o]. \tag{11}$$

The last reaction in the chain is the opening and closing of the channels. This is given as before by Eq. 1, but now (A_2R), as determined earlier from Eq. 11, can be incorporated into Eq. 1.

Solution of Eqs. 8–11 and 1

We observe that Eqs. 8 and 5 describe the hydrolysis of A as a simple form of enzymatic reaction. Segel (1988) showed that if such an enzymatic reaction fulfills the condition

$$\frac{E_T}{K_E + A_0} \ll 1, \tag{12}$$

then the system can be described as being in a quasi-steady state. Here, E_T is the total amount of acetylcholinesterase,

$$K_E = (k_2^E + k_{-1}^E)/k_1^E$$

is the half-saturation concentration, and A_0 is the initial concentration of A. Examination of Tables 1 and 2 shows that $K_E \approx \frac{1}{2} \times 10^{-3}$ M, $E_T = 6 \cdot 10^{-4}$ M and $A_0 = 2 \cdot 10^{-3}$. Thus, the ratio described in Eq. 12 is ~0.25. This value is not especially small, but still allows for the use of the quasi-steady-state approach for semi-quantitative accuracy. According to the quasi-steady state, dA/dt is given by

$$dA/dt = -\frac{k_2^E E_T \cdot A}{K_E + A}. \tag{13}$$

Examination of Table 1, and recollection of our earlier discussion, show that the initial A is large compared with K_E. Therefore, as long as the concentration of A is still higher or equal to K_E, Eq. 13 can be further simplified to become

$$dA/dt = -k_2 E_T. \tag{14}$$

The solution of Eq. 14 for A as a function of time, A_t is,

$$A_t = A_0 - k_2 E_T t. \tag{15}$$

The next process is the binding of one molecule of A to the postynaptic receptor, R. This reaction is described in Eq. 10. An exact solution of Eq. 10 requires that A varies with time, either according to Eq. 13, or as approximated by Eq. 15. Such an approach, however, results in a relatively complicated expression for (AR), and diminishes the advantage of the present approach. Moreover, Fig. 2 *A* and *C* show that A could be considered as being rather constant at the time of the build-up and the existence of (AR). Therefore, we replace A in Eq. 10 by a constant A, which is a typical value of A for the period of time under consideration. We also neglect (A_2R) and O in Eq. 7*a*. With these two simplifications, Eq. 10 may be approximated by

$$d(AR)/dt = 2k_1^R \cdot \bar{A} \cdot R_T - (AR)[\bar{A}(2k_1^R + k_2^R) + k_{-1}^R]. \tag{16}$$

We shall later use Eq. 13 or 15 to estimate the constant $\bar{A}$. Solving Eq. 16 for (AR) with the initial conditions:

$$(AR)_0 = 0 \tag{17}$$

we find that

$$(AR)_t = (b/a)[1 - \exp(-at)], \tag{18}$$

where

$$a = \bar{A}(2k_1^R + k_2^R) + k_{-1}^R; \qquad b = 2k_1^R \bar{A} \cdot R_T. \tag{19}$$

Examination of Eq. 18 shows that at longer times, $(AR)_t \rightarrow b/a$, its steady-state level, and does not decline, as it should (see Fig. 2 *C*). This behavior results from our approximate procedure, according to which, A remains constant at the value of $\bar{A}$. This, however, does not seem to create a problem, as (AR) indeed remains rather constant at its maximal value when the formation of (A_2R) takes place (see Figs. 2 *C* and *D*).

We turn now to the solution of A_2R. We note that, during the intermediate period under consideration, as a first approximation, reaction (scheme 2a) (i.e., formation of AR) is already virtually at steady-state, while reaction (scheme 2 *b*) (i.e., formation of A_2R) is not yet significant. Thus, in particular, we can write the approximate conservation relation $(AR)_{\text{total}} = AR + A_2R$.

For $(AR)_{\text{total}}$, we take the steady-state level b/a. Hence in Eq. 11, we can make the substitution $AR = (b/a) - A_2R$. This yields

$$(A_2R)_t = \frac{\alpha}{\beta}[1 - \exp(-\beta t)] \quad \text{for} \quad t < t_m, \tag{20a, b}$$

where

$$\alpha = k_2^R \cdot \bar{A} \cdot b/a = \frac{R_\perp \cdot k_2^R \cdot \bar{A}}{(1 + k_2^R/2k_1^R)}; \qquad K_R = \frac{k_{-1}^R}{k_1^R} \tag{21a}$$

and

$$\beta = 2k_{-2}^R + k_o + k_2^R \bar{A}. \tag{21b}$$

Examination of Eq. 20 shows that it has the same properties as Eq. 18. At short time, $(A_2R) = 0$, but it plateaus at longer times instead of decreasing, as it should (see Fig. 2 *D*). Hence the addition of Eq. 20 b, which restricts use of Eq. 20 a to the time interval $0 < t < t_m$ during which A_2R increases. In order to determine the decay of (A_2R), we assume that $A \rightarrow 0$ at the peak of (A_2R), $(A_2R)_m$. Examination of Fig. 2, *A* and *D* shows that this is not exactly the case, but that indeed A, at the time of $(A_2R)_m$, is a very small fraction of the initial A. Setting $A = 0$ at the time of $(A_2R)_m$ is therefore a reasonable approximation. It will be shown later (Fig. 4) that this approximation is the main source for quantitative inaccuracy in the analytical solution for the epc. However relaxing this approximation results in a more complicated and less manageable expression. Therefore, at the present time we adopt this approximation. Solving Eq. 11 with $A = 0$, gives

$$(A_2R)_t = (A_2R)_m \exp[-\gamma(t - t_m)]; \tag{22a}$$

$$\gamma = 2k_{-2}^R + k_o \quad \text{for} \quad t > t_m. \tag{22b}$$

Here, t_m is the time when $(A_2R)_t$ reaches its peak, $(A_2R)_m$. Eq. 22 describes the decay of $(A_2R)_t$; the full profile of $(A_2R)_t$ can be obtained from Eqs. 20a and 22.

We are now ready for the last process in the sequence, the opening of the channels. Since O builds up after the peak of (A_2R) is obtained, $(A_2R)_t$ of Eq. 22 is incorporated into Eq. 1 for the solution of the kinetics of channels opening. Thus,

$$dO/dt = k_o(A_2R)_m \exp[-\gamma(t - t_m)] - k_c O. \tag{23a}$$

The proper initial condition that O vanishes at $t = t_m$ is approximated by

$$Ot_m = 0. \tag{23b}$$

Because the synaptic current is proportional to the number of open channels, (Magleby and Stevens, 1972) solution of Eq. 23 will give the kinetics of the epc. Thus,

$$O_t = \frac{k_o(A_2R)_m}{k_c - \gamma}\{\exp[-\gamma(t - t_m)] - \exp[-k_c(t - t_m)]\}. \tag{24}$$

Eq. 24 shows the experimentally observed behavior of a build up of O_t followed by a decline.

A, AR, A_2R, and O, obtained using the sequential approach (Eqs. 8–11 and Eq. 1) are depicted in Fig. 3. AE is not shown in Fig. 3, because A is solved by Eq. 15. It can be seen that there is generally adequate agreement between the various components of Fig. 2 and Fig. 3. In particular, A decays to ~20% of its initial value within ~20 μs (see Figs. 2 A and 3 A). Later, the two diverge, where A diminishes faster in Fig. 3 A. The faster decline of A in Fig. 3 A results from using Eq. 15. Improvement could be obtained if A were solved using Eq. 13. However this detail is of no importance for the final shape of O, because A is assumed to drop to zero when $t = t_m$ (i.e., the time of peak, of A_2R). The build up of AR is satisfyingly similar in Figs. 2 C and 3 B, and the difference at later times does not appear to be significant for our purposes. The most noticable discrepancy is in the decay of A_2R. The accumulation of A_2R is rather adequate, but the decline is too fast in Fig. 3 C compared with Fig. 2 D. This results from the approximation made, that A drops abruptly to become zero at $t = t_m$. This approximation has been employed in order to solve the decaying phase of A_2R (see earlier discussion). The error due to the faster decline of A_2R is carried on to the decay of O_t. Fig. 4 compares O_t from Eq. 24 to that from Fig. 1 (*insert*). It is apparent that the build-up, time to peak and the peak amplitude of O_t are quite well represented by the sequential approach. However the decay of O_t is faster according to the sequential approach. Semilogarithmic plots of the decay of O_t according to the two approaches are shown in Fig. 4. The decay constants are 4.7 ms^{-1} for the sequential

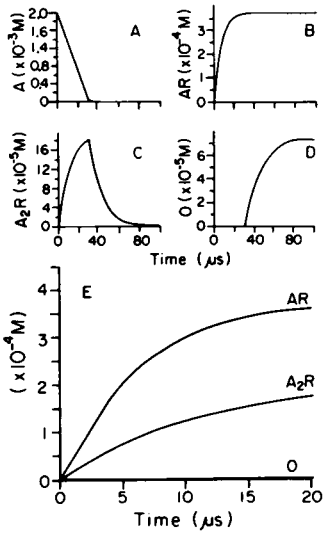

FIGURE 3 Computer simulation of A, AR, A_2R, and O using Eqs. 8–11 and then Eq. 1. Note difference in time scale of E compared with A–D. The constant $\bar{A}$ that has been employed was obtained from Eq. 15, when $t = 7$ μs.

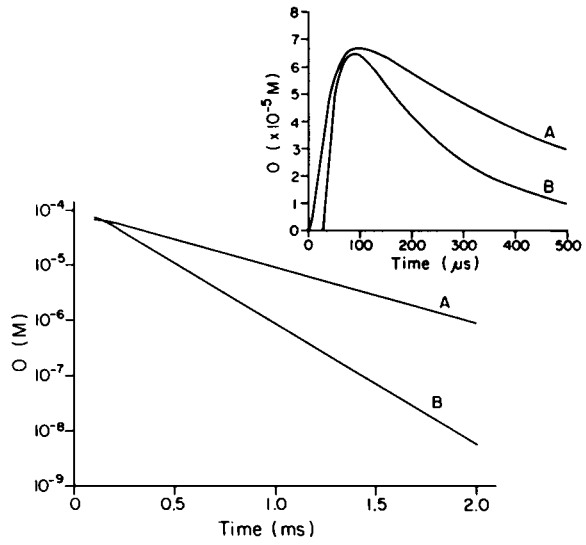

FIGURE 4 Semilogarithmic plots of the decay of O. (A), represents the continuous model, where the decay constant is 2.2 ms^{-1}; (B), represents the sequential model, the decay constant being 4.7 ms^{-1}. (*Insert*) (A) The continuous approach, i.e., as in Fig. 1. (B) The sequential approach as given by Eq. 24. The value of the constant $\bar{A}$ is obtained from Eq. 15 where the time of hydrolysis is 12 μs.

model and 2.2 ms^{-1} for the continuous one. The solution of Eqs. 8–11 and then Eq. 1 is defined for later discussion as the sequential approach.

Using the sequential approach, we can now solve for the peak amplitude of O, O_p, and the time at which O_p occurs, t_p.

The time at which O reaches its maximum, t_p, can be found by setting dO/dt to zero in Eq. 23a, and employing Eq. 24 at t_p. Thus,

$$t_p = t_m + \frac{\ln \gamma - \ln k_c}{\gamma - k_c} = t_m + \frac{\ln (\gamma/k_c)}{\gamma - k_c}. \qquad (25)$$

Evaluation of Eq. 25, using the parameters in Table 1 and setting $t_m = 30$ μs (see Fig. 2 D), gives $t_p \approx 100$ μs. Examination of Figs. 1 and 4 shows that the peak of O is obtained at ~100 μs. Thus, the agreement between Eq. 25 and the numerical solution is reasonable.

The peak amplitude of the epc, Op, can be obtained by setting dO/dt to zero in Eq. 23a and incorporating $t = t_p$ from Eq. 25. Thus,

$$O_p = \frac{k_o(A_2R)_m}{k_c} \exp\left[-\gamma\left(\frac{\ln \gamma - \ln k_c}{\gamma - k_c}\right)\right]. \qquad (26)$$

Since $\gamma \gg k_c$ (see Table 1 and Eq. 22), Eq. 26 can be simplified to

$$O_p = \frac{k_o(A_2R)_m}{k_c} \exp\left[-(\ln \gamma - \ln k_c) = \frac{k_o(A_2R)_m}{\gamma}\right] \qquad (27)$$

$(A_2R)_m$ is obtained from Eq. 20 at $t \rightarrow t_m$. Thus incorporation of Eqs. 20 and 22 into Eq. 27 gives,

$$O_p = \frac{k_o R_T k_2^R \bar{A}}{[2k_{-2}^R + k_o][(1 + k_2^R/2k_1^R) + (K_R/2\bar{A})][2k_{-2}^R + k_o + k_2^R\bar{A}]}. \quad (28)$$

SENSITIVITY ANALYSIS OF O_t

The adequacy of the sequential approach can be further tested by comparing the dependence of O_t on various parameters according to the two approaches (i.e., the sequential and the continuous approaches) (Figs. 5–8).

Dependence of the peak amplitude of *O* on *A*

The dependence of the peak amplitude of O on A can be evaluated from Eq. 28. The precise value of the peak amplitude depends strongly on the value of $\bar{A}$ that is being used in Eq. 30. However as mentioned earlier, the purpose of the present approach is to obtain, as simply as possible, an analytical expression that relates the epc, in general, and the peak amplitude, in particular, to the various underlying molecular events and their corresponding parameters. Toward this end, understanding the dependence of the peak amplitude on A is of greater importance than its exact value.

Eq. 28 shows that at low A, when

$$k_2^R\bar{A} \ll 2k_{-2}^R + k_o \quad \text{and} \quad [K_R/2\bar{A}] \gg [1 + k_2^R/2k_1^R], \quad (29a, b)$$

that is when

$$\bar{A} \ll \frac{1}{k_2^R}[2k_{-2}^R + k_o] \quad \text{and} \quad \bar{A} \ll k_{-1}^R/[2k_1^R + k_2^R], \quad (30a, b)$$

then O_p shows a sigmoidal dependence on A with an initial cooperativity of 2. For large A, when the inequalities of Eq. 30, *a* and *b* are reversed, O_p saturates at O_p^{max}, where

$$O_p^{max} = \frac{k_o R_T}{[2k_2^R + k_o][1 + k_2^R/2k_1^R]}. \quad (31)$$

Fig. 5 compares the dependence of the peak amplitude of O (according to the two approaches) on the initial concentration of A, A_0. For clarity, we reserve the symbol O_p to denote the peak amplitude of O that is obtained from the sequential approach (see Eq. 28). O_{max} is assigned to the peak amplitude of O that is obtained from the numeric solution of Eqs. 1–7 (i.e., the continuous approach). Fig. 5 shows that the two approaches show similar dependence of the peak amplitude on A_0. Examination of Eq. 31, and

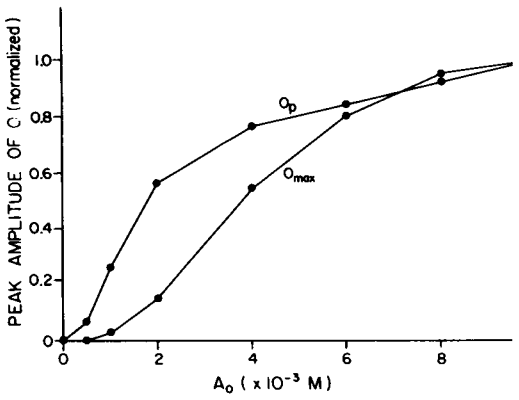

FIGURE 5 The dependence of the peak amplitude of O on the initial concentration of A, A_0. O_{max}, denotes the peak amplitude of O that is obtained from computer simulation of Eqs. 1–11, that is from the continuous approach. O_p denotes the peak amplitude of O that is obtained by employing the sequential approach. Each of the curves is normalized to its saturation value.

comparing it with O_{max} from the continuous approach, shows that the two approaches differ in the level of saturation. O_{max} saturates at $\sim 4 \cdot 10^{-4}$ M, which corresponds to $2/3\ R_T$. O_p, on the other hand, saturates at $\sim 2 \cdot 10^{-4}$ M, which corresponds to $1/3\ R_T$. This discrepancy, as others before, is due to the abrupt decline of A at $t = t_m$.

The dependence of O on the various rate constants is depicted in Figs. 6–8. In these figures, the middle curve represents the control parameters (i.e., the values that are given in Table 1).

The dependence of the epc on the rate constants of opening, k_o and closing, k_c of the channel is illustrated in Fig. 6. The resemblance between the continuous and the sequential approaches is quite adequate. At larger values of k_o (Fig. 6 *upper curve* in *A* and *B*), O declines too quickly in the sequential model (Fig. 6 *B*). This is again a result of the abrupt decay of A.

The two approaches show a similar dependence of O on the constants: k_1^R, k_2^R, k_{-1}^R, and k_{-2}^R. In particular, the sequential approach predicts reasonably well the modifications in O that are caused by varying k_1^R (Fig. 7, *A* and *B*) and k_{-1}^R (Fig. 7, *C* and *D*). Adequate resemblance is seen also when k_{-2}^R is increased (Fig. 7, *G* and *H*, *lower curves*) or when k_2^R is reduced (Fig. 7, *E* and *F*, *lower curves*). The agreement between the two approaches is less profound when k_{-2}^R is reduced; the sequential approach (Fig. 7 *H*, *upper curve*) fails to show the prolongation in the decay of O that is seen in Fig. 7 *G*, (*upper curve*). The sequential approach cannot be examined for its predictivity at higher values of k_2^R (i.e., above that of Table 1). When k_2^R increases further, the event of binding the second molecule of A to AR, that is, the

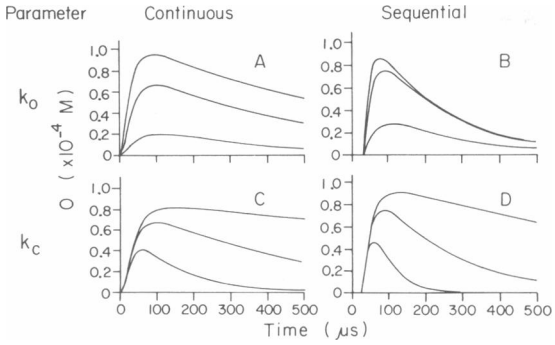

FIGURE 6 The dependence of O on the rate constants of channel opening, k_o, and closing, k_c. The dependence of the continuous model is depicted on the left hand side, while that of the sequential model, on the right hand side. In both, the middle line represents the values in Table 1. In A and B, the upper curve corresponds to a twofold increase in k_o, that is $k_o = 4 \cdot 10^4 s^{-1}$ and the lower curve to a fivefold reduction in k_o, that is $k_o = 4 \cdot 10^3 s^{-1}$. In C and D, the upper curve corresponds to a fivefold reduction in k_c, that is $k_c = 10^3 s^{-1}$, while the lower curve corresponds to a fivefold increase in k_c, that is $k_c = 2.5 \cdot 10^4 s^{-1}$.

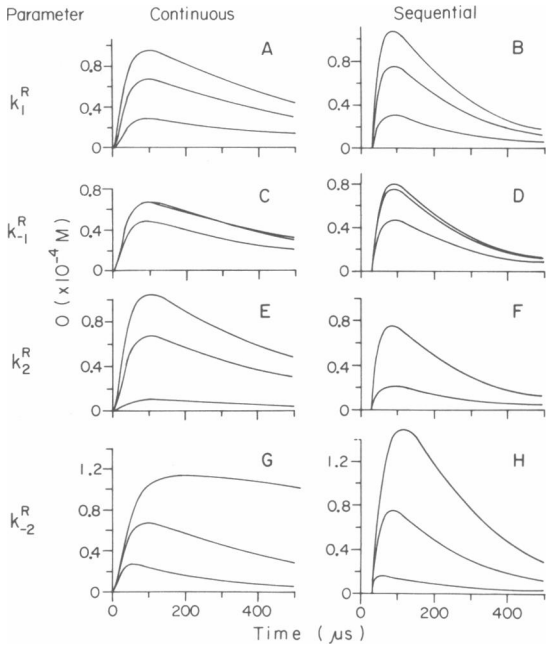

FIGURE 7 The dependence of O on the rate constants k_1^R, k_2^R, and k_{-1}^R, k_{-2}^R. As in Fig. 6, the continuous model is depicted on the left hand side and the sequential model on the right hand side. In all cases, the middle curve is that of the control values (i.e., Table 1). In A and B, the upper curve is $k_1^R = 15 \cdot 10^7 M^{-1}s^{-1}$, that is the control times 5. The lower curve is $k_1^R = 0.6 \cdot 10^7 M^{-1}s^{-1}$, that is the control/5. In C and D, the upper curve is $k_{-1}^R = 10^3 s^{-1}$, that is the control/10 and the lower curve, $k_1^R = 10^5 s^{-1}$, that is the control times 10. In E, the upper curve is $k_2^R = 6 \cdot 10^6 M^{-1}s^{-1}$ that is the control times 2, and the lower curve in E and F is $k_2^R = 3 \cdot 10^6 M^{-1}s^{-1}$, that is the control/10. In G and H, the upper curve represents $k_{-2}^R = 1 \cdot 10^3 s^{-1}$, that is the control/10 and the lower curve is $k_{-2}^R = 5 \cdot 10^4 s^{-1}$, that is the control times 5.

formation of A_2R occurs concomitantly with the formation of AR. In this case, the justification for the sequential solution of AR and A_2R is no longer valid.

In Fig. 8, the two approaches are examined to their dependence on the parameters of hydrolysis. The same pattern as before is apparent. The sequential approach predicts, with reasonable accuracy, the dependence of O on k_2^E when the rate of hydrolysis is that of the control or higher. When the rate of hydrolysis is lower (Fig. 8 *B* and *C*, *upper curves*), the abrupt decline in A on the decay phase of A_2R becomes an important source of error. Since Eq. 15, rather than Eq. 13 has been employed to solve for $\bar{A}$ in the sequential approach, there is no counterpart for k_1^E (Fig. 8 *A*) in the latter.

In conclusion, Figs. 5–8 demonstrate the ability of the sequential approach to describe the synaptic current with reasonable accuracy over a wide range of parameters.

DISCUSSION

We have presented a procedure for deriving rather simple, approximate analytical formula for the synaptic current, epc, induced by the nicotinic receptor. Obtaining an exact analytical formula is difficult because a number of processes are going on rather simultaneously. This results in a number of differential equations in which the various participating components intermingle. However, we took advantage of differences between the various rate constants, which enabled us to consider the epc as com-

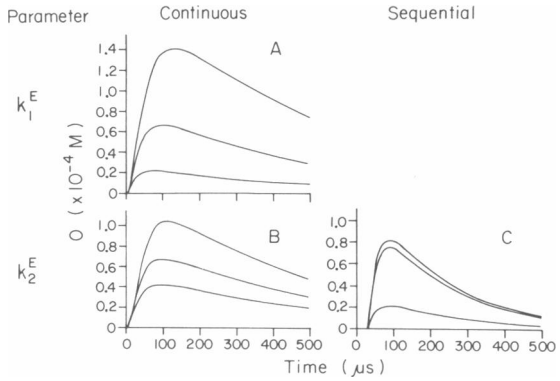

FIGURE 8 The dependence of O on the rate constants of the hydrolysis of A. In all cases, the middle curve corresponds to the control values (Table 1). In A, the upper curve reflects $k_1^E = 0.33 \cdot 10^8 M^{-1}s^{-1}$, that is the control/3.3 and the lower curve stands for $k_1^E = 2 \cdot 10^9 M^{-1}s^{-1}$, that is the control times 10. Note that there is no counterpart to k_1^E in the sequential approach. This is because A has been solved using Eq. 15. In B and C, the upper curve stands for $k_2^E = 4 \cdot 10^4 s^{-1}$, that is the control/2.7 and the lower curve stands for $k_2^E = 4 \cdot 10^5 s^{-1}$ that is the control/2.7 and the lower curve stands for $k_2^E = 4 \cdot 10^5 s^{-1}$, that is the control times 2.7.

posed of several processes occurring in sequence rather than simultaneously. As a result, we were able to develop the set of approximations that generated the formula for the synaptic current.

Our sequential solution can be compared with the earlier work of Magleby and Stevens (1972). In both cases, the decline in the synaptic current is attributed to k_c. Owing to a lack of data in 1972, Magleby and Stevens developed an analytical formula for the decline of the epc, only. We have been able to employ the data that have accumulated in the past 15 years to describe the entire epc analytically.

It is illuminating to use the analytical solution in examining the contribution of various parameters to the synaptic current. As was shown by Magleby and Stevens (1972), at large t, the decline of the synaptic current is determined mainly by k_c, the rate constant of channel closing. However it should be emphasized that even with extremely fast hydrolysis, k_c is not the only parameter that determines the decay of the epc. This becomes evident by comparing the continuous (Fig. 4 *A*) with the sequential (Fig. 4 *B*) models. According to both, the decay of the epc is determined mainly by k_c. Because we used in both $k_c = 5 \cdot 10^3\ s^{-1}$, we would expect the same decay rate. Yet the decay constant of O in the continuous model is slower ($2.2 \cdot 10^3 s^{-1}$). This slower decay reflects the contribution of the decay of the tail A_2R to the general decay of O. Another major contribution to the decline of O is evident in Fig. 7 *G*. Reduction of k^R_{-2}, the rate constant of dissociation of A from A_2R, strongly prolongs the decay of O.

It is also interesting to note that most of the acetylcholine that has been released into the synaptic cleft is being hydrolysed even before having a chance to bind the receptor. This view is somewhat different from that expressed by Wathey et al. (1979), in which acetylcholine binds first to the receptors and then is quickly hydrolyzed.

The parameters that determine the time to peak of the epc can be evaluated from Eq. 25. These are not only the rates of opening, k_o, and closing, k_c, of the channel, but also the rate of dissociation of A from A_2R, k^R_{-2}. Fig. 6, *A* and *C* and Fig. 7 *G* confirm this conclusion.

Insight into the molecular events underlying the epc can be obtained from the dependence of the peak amplitude of O on A. It is this dependence that reflects the number of transmitter molecules that invoke the opening of a single channel.

A systematic analysis of Eqs. 23–25 and 28, can provide means to estimate the values of the various parameters that are involved in generating the epc. Reassurance to such an approach comes from the reasonable agreement between the sensitivity of the continuous and the sequential approaches to the variation of the parameters. The resemblence of the two approaches in a wide range of parameters suggests that the sequential approach is also useful if the values of the parameters given in Table 1 are altered to some extent.

The present approach utilizes the transient synaptic current to study the underlying mechanisms and the dynamics of the single nicotinic channel. This is totally different from the steady-state approach (see Colquhoun and Hawkes, 1983; Colquhoun and Sakmann, 1985; Colquhoun and Ogden, 1988), and the two approaches can complement each other. There are some parameters which are easier evaluated from steady-state measurements and others from the transient synaptic currents. For example, when desensitization is involved, studies of transients are advantageous. However until recently, study of transient currents under various experimental conditions were technically very difficult. Recently, Franke et al. (1987) have developed a procedure which enables short application of transmitter. This will undoubtedly advance the use of transient measurements to assess parameters which are difficult to evaluate otherwise.

Finally, the present solution was carried out using the mechanism and parameters of the nicotinic system. Even within this framework, improvements are required. For example, a better approximation of the decaying phase of A_2R will improve accuracy. Moreover, the sequential approach might partially collapse under some conditions. One such case would be if the rate of removal of the transmitter were slow compared with its binding to the receptor. Another example would be if the various stages of the closed channel (here, AR and A_2R) were to occur too closely in time, and so could not be treated sequentially.

We believe that the present sequential analysis is of general importance, and can be extended to describe other, as yet, poorly understood synaptic currents. The close resemblance of both the sequential and the continuous simulations to the experimental results provide confidence in the validity of this approach.

We thank L. A. Segel and Stewart W. Jasloye for careful reading and significant contribution to the development of this manuscript. Computer programming was performed by Gilad Hovav.

Received for publication 11 April 1988 and in final form 14 November 1988.

REFERENCES

Anderson, C. R., and C. F. Stevens. 1973. Voltage clamp analysis of acetylcholine produced end-plate current fluctuations at frog neuromuscular junction. *J. Physiol. (Lond.).* 235:655–691.

Bernard, E. A., T. H. Chiu, U. Uedrzejcyck, C. W. Porter, and U. Wieckowski. 1973. Skeletal muscles and their nerve junctions. *In* Drug Receptors. H. P. Rang, editor. MacMillan Journals Ltd., London. 225–240.

Colquhoun, D. 1975. Mechanisms of drug action at the voluntary muscle endplate. *Annu. Rev. Pharmacol.* 15:307–320.

Colquhoun, D., and A. G. Hawkes. 1983. The principles of the stochastic interpretation of Ion-channel mechanisms. *In* Single-Channel Recording. B. Sakmann and E. Neher, editors. Plenum Publishing, Corp., New York.

Colquhoun, D., and D. C. Ogden. 1988. Activation of ion channels in the frog end-plate by high concentrations of Acetylcholine. *J. Physiol. (Lond.).* 395:131–159.

Colquhoun, D., and Sakmann, B. 1985. Fast event in single-channel currents activated by acetylcholine and its analogues at the frog muscle end-plate. *J. Physiol. (Lond.).* 369:501–557.

Franke, Ch., H. Hatt, and J. Dudel. 1987. Liquid filament switch for ultra-fast exchanges of solutions at excised patches of synaptic membrane of crayfish muscle. *Neurosc. Lett.* 77:199–204.

Gage, P. W., and R. N. McBurney. 1975. Effects of membrane potential temperature and neostigmine on the conductance change caused by a quantum of acetylcholine at the toad neuromuscular junction. *J. Physiol. (Lond.).* 244:385–407.

Kordas, M. 1977. On the role of junctional cholinesterare in determining the time course of the end-plate current. *J. Physiol. (Lond.).* 270:133–150.

Land, B. R., W. V. Harris, E. E. Salpeter, and M. M. Salpeter. 1984. Diffusion and binding constants for acetylcholine derived from the falling phase of miniature endplate currents. *Proc. Natl. Acad. Sci. USA.* 81:1594–1598.

Magleby, K. L., and C. F. Stevens. 1972. A quantitative description of end-plate currents. *J. Physiol. (Lond.).* 223:173–197.

Matthews-Bellinger, U., and M. M. Salpeter. 1978. Distribution of acetylcholine receptors at frog neuromuscular junctions with a discussion of some physiological implications. *J. Physiol. (Lond.).* 279:179–213.

McLachlan, E. M., and A. R. Martin. 1981. Non-linear summation of end-plate potentials in the frog and mouse. *J. Physiol. (Lond.).* 811:307–324.

Miledi, R., P. C. Mollnaar, and R. L. Polak. 1984. Acetylcholinesterase activity in intact and homogenized skeletal muscle of the frog. *J. Physiol. (Lond.).* 349:663–686.

Rosenberry, T. L. 1975. Acetylcholinesterase. *Adv. Enzymol.* 43:103–218.

Rosenberry, T. L. 1979. Quantitative simulation of endplate currents at neuromuscular junctions based on the reaction of acetylcholine with acetylcholine receptor and acetylcholinesterase. *Biophys. J.* 26:263–290.

Rosenberry, T. L., and S. A. Bernhard. 1972. Studies of catalysis by acetylcholinesterase. Synergistic effects of inhibitors during the hydrolysis of acetic acid esters. *Biochemistry.* 11:4309–4321.

Segel, L. A. 1988. On the validity of the steady state assumption of enzyme kinetics. *Bull. Math. Biol.* 50:579–593.

Sheridan, R. E., and H. A. Lester. 1977. Rates and equilibria at the acetylcholine receptor of Electrophorus electroplaques. *J. Gen. Physiol.* 70:187–219.

Steinbach, U. H., and C. F. Stevens. 1976. Neuromuscular transmission. *In* Frog Neurobiology. R. Llinas and W. Precht, editors. Springer Verlag, Inc., New York. 33–92.

Wathey, U. C., M. M. Nass, and H. A. Lester. 1979. Numerical reconstruction of the quantal event at nicotinic synapses. *Biophys. J.* 27:145–164.